Journal of Molecular Spectroscopy **202,** 213–222 (2000)
doi:10.1006/jmsp.2000.8139, available online at http://www.idealibrary.com on IDEAL®

The Rotational Analysis of the $A^2\Pi_r$–$X^2\Sigma^+$ Band System of MgBr

T. Hirao,[1] B. Pinchemel,[2] and P. F. Bernath[1,3]

Department of Chemistry, University of Waterloo, Waterloo, Ontario, Canada N2L 3G1

Received December 22, 1999; in revised form April 17, 2000

The $A^2\Pi_r$–$X^2\Sigma^+$ emission spectrum of the magnesium monobromide radical, MgBr, has been recorded with a Fourier transform spectrometer modified to record double-sided interferograms. The emission spectra of the $\Delta v = -2, -1, 0, +1$ bands were generated in a microwave discharge of a mixture of argon and vaporized $MgBr_2$. The $\Delta v = 0$ and -1 bands were rotationally resolved, but the F_2 spin component ($A^2\Pi_{3/2}$) in the (1, 1), (1, 2) and vibrational bands with $v' > 1$ were missing in our spectra because of a strong predissociation in the *A* state. The molecular constants in both electronic states were determined for the two bromine isotopomers. The r_0 bond length in the *A* state is about 2.327 Å, which is about 0.02 Å shorter than in the ground state. Franck–Condon factors were calculated from the Rydberg–Klein–Rees potentials, and they reproduce the observed relative intensities of the bandheads. An upper limit for the dissociation energy (D_0^0) was obtained as 26 268.4 cm^{-1}, based on the absence of the energy level with $v = 1$, $A^2\Pi_{3/2}$, $J = 1.5$ in our spectrum.

I. INTRODUCTION

Predissociation resonance is an interesting perturbation in the spectra of diatomic molecules and many studies of this phenomenon have been reported (*1*). This phenomenon results when a bound potential curve is intersected by a repulsive potential curve. For example, the $C^2\Pi$ state of the magnesium monohydride radical (MgH) is predissociated by a dissociative $^2\Sigma^+$ state and as a result the rotational structure in the 0–0 band of the *C*–*X* transition around 243 nm is suddenly "cutoff" (*1*, *2*).

In the magnesium halide family, MgCl and MgBr are also reported to have a predissociated $^2\Pi$ state, which lies about 26 000 cm^{-1} above the ground state. Although the $A^2\Pi$–$X^2\Sigma^+$ transition of MgCl was known early this century (*3*), it is only recently that Rostas *et al.* (*4*) demonstrated that the *A* state is predissociated. They found that the laser-induced fluorescence (LIF) spectra showed a sudden cutoff at $v_A = 7$. In addition, it was found that the spin–orbit coupling constant, A_{SO}, and the vibrational intervals, $\Delta G_{v+1/2}$, in the *A* state have a strong *v*-dependence. They also carried out a rotational analysis of the (0, 0), (0, 1), and (0, 2) bands observed previously by Singh *et al.* (*5*) and corrected the previous assignments (*5*). They found that the lambda-type doubling constant *p* and the spin–orbit constant are positive in the *A* state, although the lambda-doubling should be negative due to a higher lying $^2\Sigma^+$ state (*6*). All of these unusual features derive from a continuum $^2\Pi_i$ state, which causes a predissociation in the *A* state (*4*).

The anomalous lambda-doubling in MgCl can be explained by a mixing of the $^2\Pi_i$ state with the $A^2\Pi_r$ state. The inverted $^2\Pi$ state is characterized by a π electron (or more correctly an electron hole) which originates from an atomic halogen Cl orbital, whereas the regular *A* state is characterized by a π electron in a metal-centered orbital. Because of the mixing of a regular *A* state and an inverted $^2\Pi$ state, the lambda-doubling is influenced both by positive A_{SO} of the "pure" *A* state and by the negative A_{SO} of the inverted $^2\Pi$ state. This explanation also accounts for the variation of A_{SO} with the halogen atom of the Mg*X* (*X* = F, Cl, and Br) series, in which A_{SO} increases strongly from MgF (37 cm^{-1} (*7*)), MgCl (54 cm^{-1} (*4*)), to MgBr (120 cm^{-1} (*8*)). This behavior is to be compared to the $A^2\Pi$ states in the Ca*X*, Sr*X*, and Ba*X* (*X* = F, Cl, Br, and I) radicals for which A_{SO} changes only slightly when the halogen atom changes (*8*). Considering that the spin–orbit coupling constant of Mg^+ is relatively small and that of the halogen atom increases from F to I (*6*), this variation of A_{SO} of Mg*X* shows an increase in the contribution of a halogen atom to the electronic configuration of the *A* state. These conclusions (*4*) are also supported by more sophisticated theoretical calculations (*9*), and it may be expected that MgBr would have a larger predissociation in the *A* state.

The first spectroscopic detection of the MgBr radical was reported by Olmsted at the beginning of the 20th century (*3*). In 1928, Walters and Barrett obtained absorption spectra of MgBr in the same wavenumber region (*10*). Morgan made the first vibrational assignment for the *A*–*X* transition and attributed this system to the $A^2\Pi$–$X^2\Sigma^+$ transition (*11*).

Harrington observed the *A*–*X* and $C^2\Pi$–$X^2\Sigma^+$ transitions in

Supplementary data for this article are available on IDEAL (http://www.idealibrary.com) and as part of the Ohio State University Molecular Spectroscopy Archives (http://msa.lib.ohio-state.edu/jmsa_hp.htm).

[1] To whom correspondence should be addressed. E-mail: thirao@sciborg.uwaterloo.ca, bernath@UWaterloo.ca.

[2] Permanent address: Laboratoire de Physique des Lasers, Atomes et Molécules, UMR CNRS 8523, Centre d'Etudes et de Recherches Lasers et Applications, Université des Sciences et Technologies de Lille, 59655, Villeneuve d'Ascq Cedex, France.

[3] Also: Department of Chemistry, University of Arizona, Tucson, Arizona 85721.

0022-2852/00 $35.00

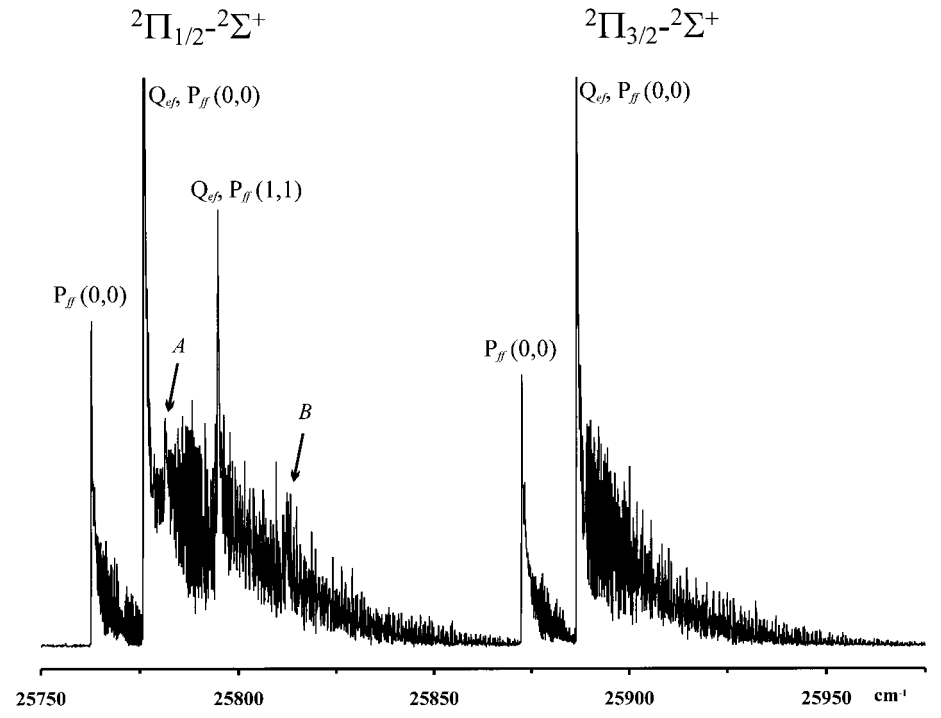

FIG. 1. Overview of the $\Delta v = 0$ bands of the $A^2\Pi$–$X^2\Sigma^+$ transition of MgBr. *A* and *B* indicate the P_{ff} (1, 1) and Q_{ef}, P_{ff} (2, 2) bandheads, respectively.

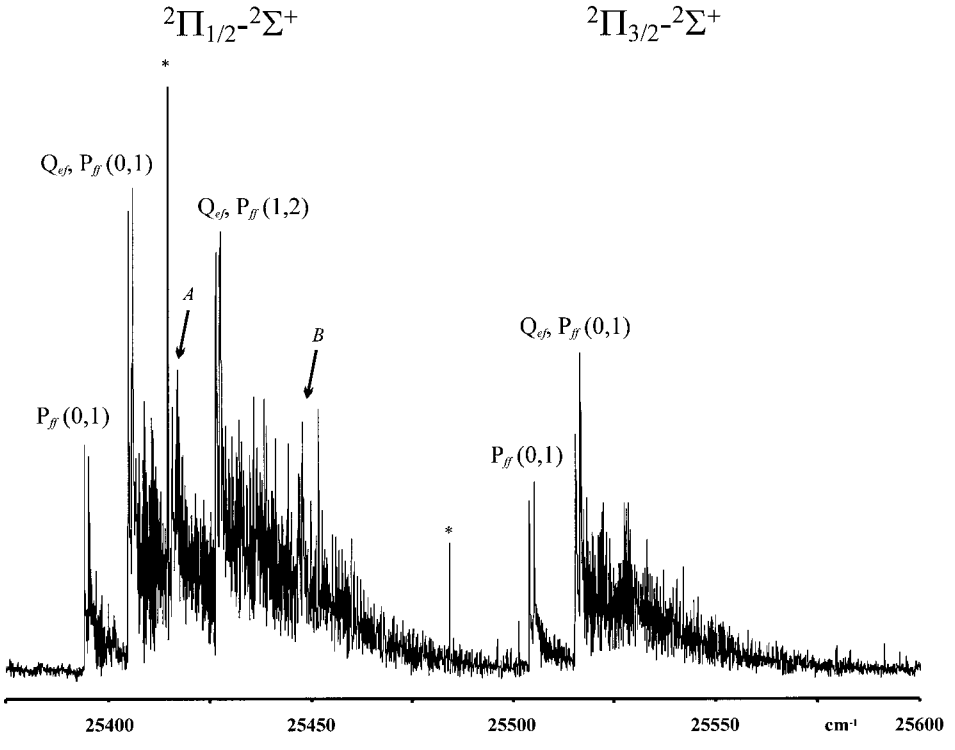

FIG. 2. Overview of the $\Delta v = -1$ bands of the $A^2\Pi$–$X^2\Sigma^+$ transition of MgBr. *A* and *B* indicate P_{ff} (1, 2) and Q_{ef}, P_{ff} (2, 3) bandheads, respectively. The lines denoted by asterisks are probably bromine atomic lines.

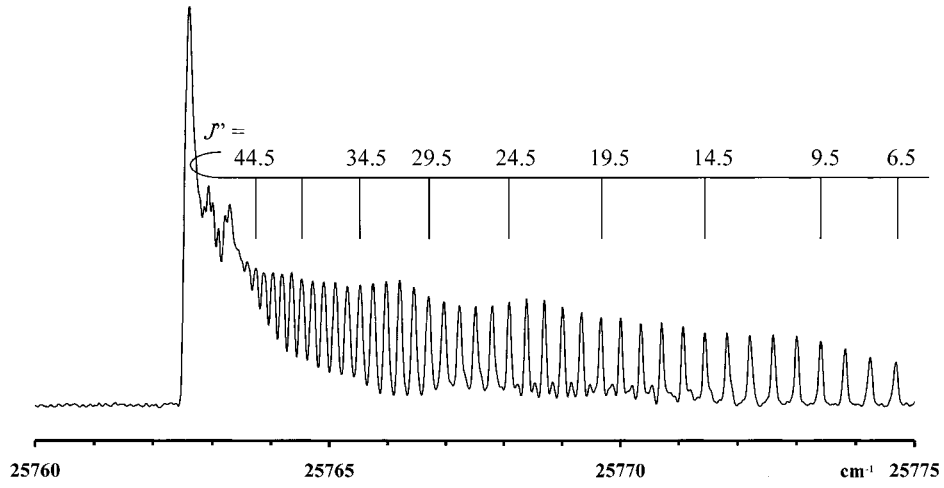

FIG. 3. A portion of the P_{ff} branch of the F_1 spin component of the (0, 0) band. Several small lines around 25 770 cm^{-1} perhaps belong to the minor Mg isotopomers.

absorption and noted a predissociation in the *A–X* system for the first time (*12*). The spectra were measured with a high-temperature furnace and contained $\Delta v = -2, -1, 0, +1$ vibrational sequences up to $v_A = 5$. He found that the (3, 3), (4, 4), and (5, 5) Q_{ef} bandheads for the F_1 spin component and the (1, 1) and (2, 2) heads for the F_2 spin component are diffuse, less intense than expected, and shifted from their expected positions. It was not possible to detect $v_A \geq 3$ for the F_2 spin component. After a partial rotational analysis of the (0, 0) band by Patel and Patel (*13*), Puri and Mohan observed thermal emission spectra of the *A–X* bands up to $v_A = 5$ and saw the $\Delta v = -3$ and $+4$ sequences. They used a King furnace at a temperature of about 2200°C (*14*) and also pointed out similar band features as Harrington (*12*).

Recently, Sadygov *et al.* (*15*) carried out *ab initio* calculations on MgBr and compared the results with a medium-resolution LIF spectrum of the *A–X* band system. They obtained Q_{ef} and P_{ff} bandheads for the $A^2\Pi_{3/2}$, $v_A = 0, 1$ levels, but suggested that the $A^2\Pi_{3/2}$, $v_A = 1$ level was partially predissociated because it had unreasonably weak

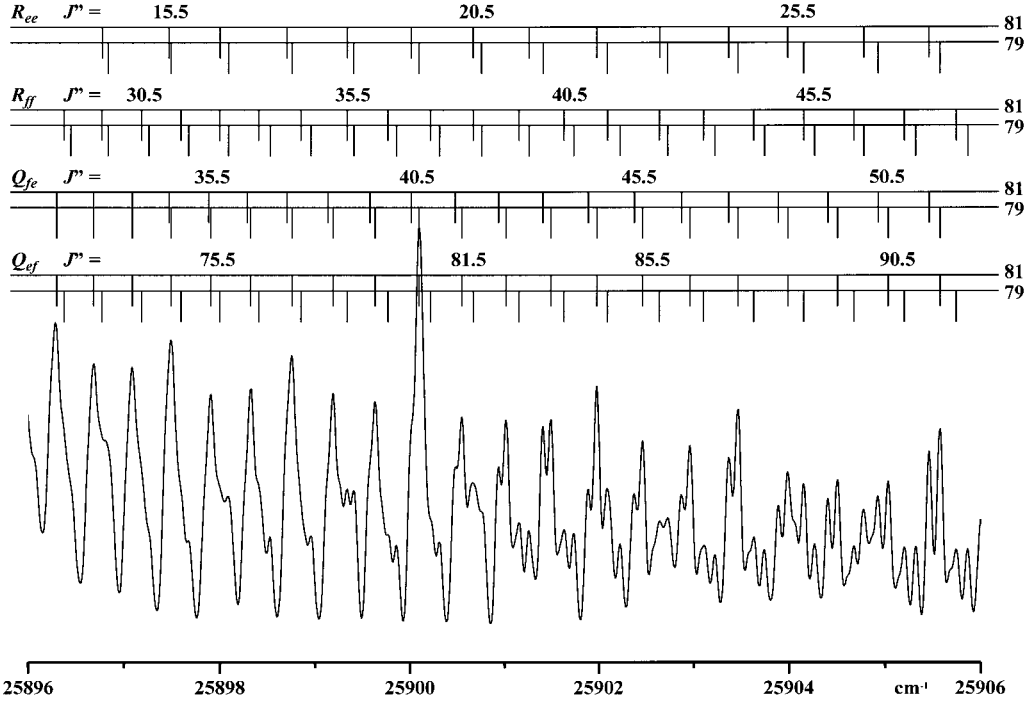

FIG. 4. A portion of the F_2 spin component of the (0, 0) band.

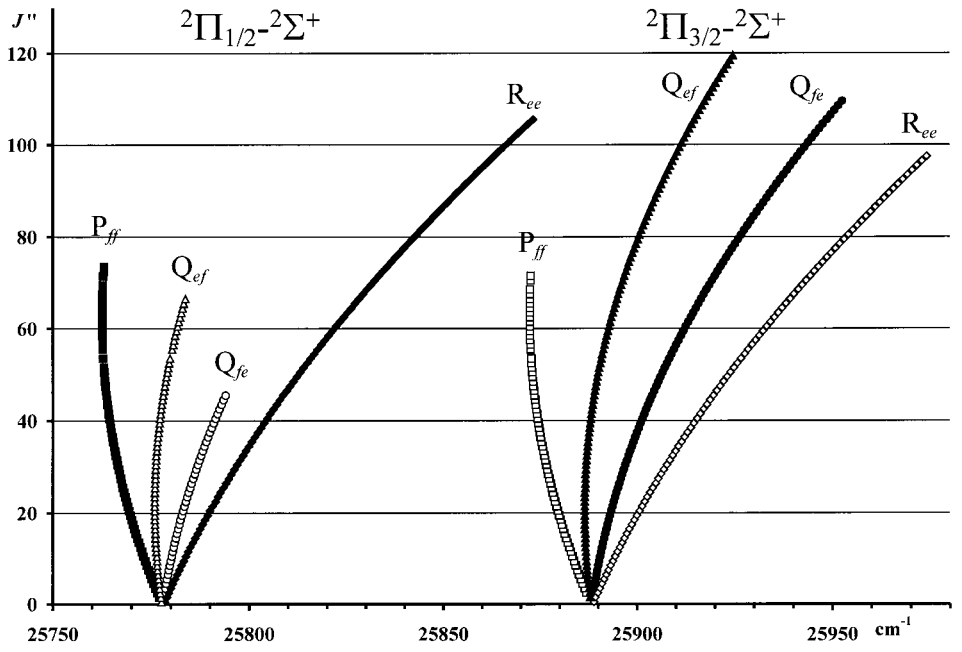

FIG. 5. Fortrat diagram of the (0, 0) band. Note that for simplicity the P_{ee} and R_{ff} branches are excluded in this figure.

fluorescence. On the other hand, P_{ff} and P_{ee} bandheads for $A^2\Pi_{1/2}$, $v_A = 0$, 1 levels were detected, but only a very weak P_{ee} bandhead was obtained for the $A^2\Pi_{1/2}$, $v_A = 2$ level. The Ω dependence of the predissociation is caused by the relatively small spin–orbit coupling constant, $\sim +100$ cm^{-1} in the A state, whereas the dissociative $^2\Pi_i$ state has a large negative value, ~ -2200 cm^{-1} (*15*). As a result, the crossing of the potential curves for $\Omega = \frac{3}{2}$ happens about 1200 cm^{-1} lower than that for $\Omega = \frac{1}{2}$. Sadygov *et al.* (*15*) also found an additional indirect predissociation resonance for $v = 3$, 4 of the $\Omega = \frac{1}{2}$ spin component by mixing with $v = 3$, 4 of the $\Omega = \frac{3}{2}$ spin component by the normal *S*-

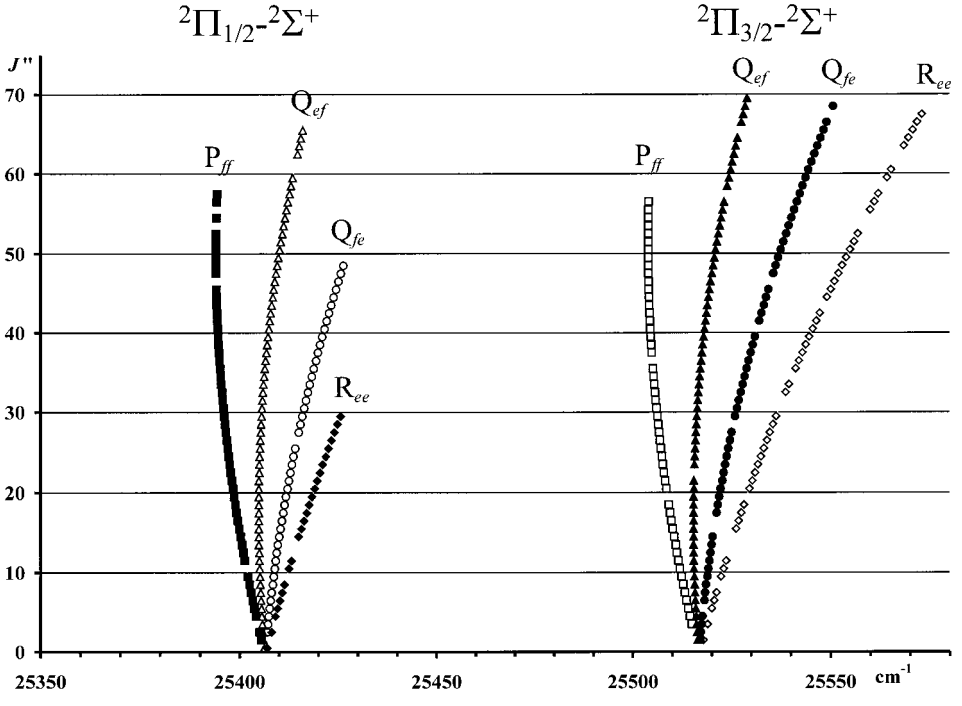

FIG. 6. Fortrat diagram of the (0, 1) band. Note that for simplicity the P_{ee} and R_{ff} branches are excluded in this figure.

TABLE 1
Molecular Constants of MgBr

	$Mg^{79}Br$	$Mg^{81}Br$
$A^2\Pi_r$ state, $v = 0$		
T_0'	25833.01403(98)	25832.98315(98)
A_0'	110.7006(17)	110.6975(18)
$A_{D0}' \times 10^4$	-5.2452(100)	-5.0327(100)
B_0'	0.16973390(59)	0.16875687(54)
$D_0' \times 10^7$	1.32255(119)	1.3048(59)
p_0'	0.022647(62)	0.021806(56)
$p_{D0}' \times 10^6$	-0.959(23)	-1.222(20)
$X^2\Sigma^+$ state, $v = 0$		
T_0''	0.0(fixed)	0.0(fixed)
B_0''	0.1658547742(39)	0.1649015936(56)
$D_0'' \times 10^7$	1.30650(96)	1.2823(58)
$\gamma_0'' \times 10^3$	5.947644(23)	5.913511(21)
$\gamma_{D0}'' \times 10^9$	-8.1(29)	-4.8(18)
$v = 1$		
T_1''	371.4838(23)	370.4096(24)
B_1''	0.1649350142(50)	0.1639897500(60)
$D_1'' \times 10^7$	1.2976(46)	1.2884(64)
$\gamma_1'' \times 10^3$	5.861065(18)	5.827731(19)

1. In cm^{-1} units. The numbers in the parentheses indicate the standard error in the last significant digits.

uncoupling interaction followed by a strong interstate interaction between the *A* state and the continuum $^2\Pi_i$ state. This indirect interaction becomes important as the quantum number *J* increases and as the spin–orbit constant decreases for the higher vibrational levels of the *A* state.

Walker and Gerry examined the Fourier transform microwave (FTMW) spectrum of MgBr and obtained rotational transitions for a few low-lying rotational levels of the ground state (*16*). On the basis of the r_e value and the hyperfine structure, they concluded that the unpaired electron is located on the Mg atom and that the Mg–Br bond is almost completely ionic in the ground state.

Apart from a partial rotational analysis (*11*), there is almost no rotational information available for the *A* state. In this study, we recorded the rotationally resolved *A–X* transition of MgBr by using a Fourier transform spectrometer. The (0, 0) and (0, 1) vibrational bands were rotationally assigned. We also obtained several weak bandheads up to $v_A = 2$ and $v_X = 4$. By considering Harrington's results (*12*), we could determine improved vibrational constants and RKR potentials for the $A^2\Pi$ and $X^2\Sigma^+$ states.

II. EXPERIMENTAL

A few tens of grams of $MgBr_2$ (Aldrich, 99.9%) precursor were placed in a quartz tube. The precursor was heated up to more than 400°C by a heating tape wrapped around the tube. A slow flow of Ar buffer gas at a pressure of 1.5 Torr carried the $MgBr_2$ vapor into the microwave discharge region. One hundred watts of power at 2.45 GHz was applied to the microwave cavity. The discharge glow was focused onto the emission port of the FTS with a CaF_2 lens.

All of the spectra of MgBr were recorded with the modified Bruker IFS 120HR Fourier transform spectrometer (FTS) at University of Waterloo (*17*). The spectrometer was recently modified to record double-sided interferograms, in order to eliminate lineshape problems associated with the phase correction. We also made a new emission port directly in front of the entrance aperture so that a single lens can be used to focus emission into the spectrometer. Finally we attached a photomultiplier tube to the "back parallel exit." This was very important in order to improve sensitivity in the visible and ultraviolet regions because the numerous reflections from the aluminum mirrors in the sample chamber and the detector compartment reduce the signal intensity. During the observation we did not evacuate the spectrometer, which caused all of the wavenumbers to be influenced by the refractive index of air. Because of this, we had to convert all of the measurements to vacuum wavenumbers, as discussed in the next section.

A visible quartz beamsplitter was used to record the spectra. Many strong lines such as magnesium atomic lines near 19 000 cm^{-1} (*18*) were located near our spectral region. These strong atomic lines could reduce our signal-to-noise ratio. To minimize the influence of extraneous emission, we used a 450-nm blue-pass filter (Corion, LS-450) which cuts the light below 22 200 cm^{-1}. The spectra were measured from 24 000 to 27 400 cm^{-1} because there were no strong atomic lines detected in this spectral range. The emission spectra were accumulated for 10 scans at a spectral resolution of 0.05 cm^{-1}. Norton–Beer–weak was selected as the apodization function. The zero-filling factor was 2, and the dispersion was approximately 0.015 cm^{-1} per data point.

III. RESULTS

We have obtained the $\Delta v = -2, -1, 0, +1$ vibrational sequences in the 24 000–26 300 cm^{-1} region. These vibrational sequences were almost evenly separated by 350 cm^{-1}. Among these, the $\Delta v = -1$ and 0 bands such as (0, 1) and (0, 0) were strong and rotationally resolved but only bandheads were available for the $\Delta v = -2$ and $+1$ bands. Overview spectra of the $\Delta v = 0$ bands of the *A–X* transition are shown in Fig. 1. The F_1 spin component ($A^2\Pi_{1/2}$–$X^2\Sigma^+$, left part) contains five bandheads up to $v_A = 2$, namely P_{ff} (0, 0), Q_{ef} (0, 0), P_{ff} (1, 1), Q_{ef} (1, 1), and Q_{ef} (2, 2). On the other hand, the F_2 spin component ($A^2\Pi_{3/2}$–$X^2\Sigma^+$, right part) con-

TABLE 2
List of the Observed Bandhead Positions

$v'\backslash v''$		0	1	2	3	4
(1) F_1 spin component ($A^2\Pi_{1/2}$-$X^2\Sigma^+$)						
	P_{ff}	25762.66 [0.00]	25394.06 [+1.10]	25027.37 [+2.12]	-	-
0	P_{ee}	25775.80 [0.00]	25404.73 [+1.04]	-	-	-
	Q_{ef}	25775.93 [0.00]	25404.85 [+1.04]	25036.37 [+2.10]	-	-
	P_{ff}	-	25781.26 [0.00]	25415.52 [+1.04]	25051.61 [+2.05]	-
1	P_{ee}	26165.33 [-1.11]	25794.53 [0.00]	25426.27 [+1.05]	-	-
	Q_{ef}	26165.64 [-1.26]	25794.70 [0.00]	25426.36 [+1.01]	25060.67 [+2.01]	-
2	Q_{ef}	-	26180.34 [-1.15]	25812.22 [0.00]	25446.65 [+0.93]	25083.76 [+1.86]
(2) F_2 spin component ($A^2\Pi_{3/2}$-$X^2\Sigma^+$)						
	P_{ff}	25872.35 [0.00]	25503.91 [+1.11]	25137.34 [+2.09]	-	-
0	P_{ee}	25886.36 [0.00]	25515.26 [+1.04]	-	-	-
	Q_{ef}	25886.50 [0.00]	25515.37 [+1.18]	25146.89 [+2.06]	-	-
1	Q_{ef}	26266.7 [-1.6] [c]	25896.0 [0.0] [b]	25527.6 [+1.2] [b]	25149.1 [+2.1] [c]	-
2	Q_{ef}	-	26265.8 [-1.8] [c]	25897.6 [0.0] [b]	25532.2 [+0.7] [b]	-

[a] All numbers are in cm^{-1}. The number in square brackets indicates the isotope shift, $\nu(Mg^{81}Br)-\nu(Mg^{79}Br)$.
[b] Measured by Ref. *12*. Used in our fit after a calibration. See text.
[c] Measured by Ref. *12*, but neither calibrated nor included in our fit. See text.

tains only the (0, 0) band. Note that all bandheads of the bromine isotopomers, $^{24}Mg^{79}Br$ and $^{24}Mg^{81}Br$, overlap each other because the molecular constants of each isotopomer are very similar. Additionally, all of the Q_{ef} bandheads almost overlap with the P_{ee} bandheads, because the splitting between these two heads is determined by the small spin–rotation interaction in the ground state. The $\Delta v = -1$ region has a similar appearance (Fig. 2), except that there are double bandheads for each feature because of the bromine isotope splitting. These features agree with the recent medium-resolution LIF spectra (*15*).

Figure 3 illustrates a portion of the P_{ff} (0, 0) branch of the F_1 spin component. Typical linewidths for the P_{ff} (0, 0) branch in both F_1 and F_2 spin components were 0.08 cm^{-1}, and the signal-to-noise ratio was about 100. In these bands, there was no significant bromine isotopic shift observed. However, in the nearly final stage of the analysis, we found that high J transitions of the other branches such as Q_{fe} and R_{ee} showed some isotopic shifts (Fig. 4), and we could thus separate the two bromine isotopomers in our fitting procedure.

Spectral line positions were measured by using the program PC-DECOMP. Because the spectrometer was not evacuated, all line positions had to be corrected for the refractive index of air (*19*, *20*). We assumed that the single-mode He–Ne laser emission occurs exactly at 15 798 cm^{-1} in vacuum. If the laser emits in "standard air," which means dry air at 760 Torr and 15°C laboratory temperature (*19*, *20*), the actual emission will be shifted to the "air wavenumber" ($=1/\lambda_{air}$) 15 803.7725 cm^{-1} (*21*) by the refractive index of air at 15 798 cm^{-1}, $n_{He-Ne} = 1.00027657$. If the wavenumber of the internal He–Ne laser for the FTS in air is also set to exactly 15 798 cm^{-1}, the sampled movement of the moving mirror in the spectrometer is at its real distance multiplied by n_{He-Ne}. Hence, the interferogram, when Fourier-transformed, gives air wavenumbers divided by n_{He-Ne}, and thus the observed scale of wavenumbers, $\tilde{\nu}_{ex}$, will be simply

TABLE 3
Vibrational and Spin–Orbit Constants of $Mg^{79}Br$

		T_e	ω_e	$\omega_e x_e$
$X^2\Sigma^+$	Obs. [1]	0	374.238(2)	1.381(4)
	Obs. [2]	0	373.8	1.43
	Calc. [3]	0	365.9	1.72
$A^2\Pi_r$	Obs. [1]	25824.31(8)	392.76(18)	3.60(6)
	Obs. [3]	25823.0	394.3	2.30
	Calc. [3]	25362.8	397.4	2.83

[1] This work. Numbers in parentheses indicate the standard deviation for last significant digit.
[2] Taken from Ref. *8*.
[3] Medium-resolution LIF spectra and calculated results at the level of SA-MCSCF/SOCI were taken from Ref. *15*.

TABLE 4
Franck–Condon Factors of the $A^2\Pi$–$X^2\Sigma^+$ Transition of MgBr

v'\v"	0	1	2	3	4
0	0.9268 [a]	0.0693 [a]	0.0035 [c]	0.0004	0.0001
1	0.0704 [d]	0.7610 [b]	0.1513 [b]	0.0146 [d]	0.0020
2	0.0026	0.1587 [d]	0.5643 [b]	0.2285 [b]	0.0366 [d]

a) Observed and rotationally assigned.

b) Only the F_1 spin component was detected and some parts of this were rotationally resolved.

c) Band heads of the F_1 and F_2 spin components were detected.

d) Only band head of the F_1 spin component was detected.

$$\tilde{\nu}_{ex} = \tilde{\nu}_{air}/n_{He\text{–}Ne} = \tilde{\nu}_{vac} \times n/n_{He\text{–}Ne}, \quad [1]$$

where $\tilde{\nu}_{air}$ is an air wavenumber and $n = n(\tilde{\nu}_{vac})$ is the refractive index of air at the vacuum wavenumber $\tilde{\nu}_{vac}$ (*19, 20*). For the purpose of calculating vacuum wavenumbers from $\tilde{\nu}_{ex}$, we calculated the observed wavenumbers ($\tilde{\nu}_{ex}$) from $\tilde{\nu}_{vac}$ at 3000 data points evenly separated by 10 cm^{-1} from 0 to 30 000 cm^{-1}. Using the calculated values, a least-squares fit was performed using a simple polynomial model for the relationship between $\tilde{\nu}_{ex}$ and the calculated vacuum wavenumbers, $\tilde{\nu}_{vac}$, and we obtained

$$\Delta = \tilde{\nu}_{ex} - 15\,000, \quad [2]$$

$$\delta = -6.619702 \times 10^{-3} + 6.7274390 \times 10^{-6} \times \Delta + 7.367955 \times 10^{-10} \times \Delta^2 + 1.864215 \times 10^{-14} \times \Delta^3 + 1.22781 \times 10^{-19} \times \Delta^4 + 2.46704 \times 10^{-24} \times \Delta^5 + 2.8993 \times 10^{-29} \times \Delta^6, \quad [3]$$

$$\tilde{\nu}_{vac} = \tilde{\nu}_{ex} - \delta. \quad [4]$$

This formula is effective in the wavenumber region from 0 to 30 000 cm^{-1}. The error caused by this conversion is less than 2×10^{-6} cm^{-1} throughout the covered wavenumber region, assuming Edlén's formula reproduces the refractive index of air with a precision of 2×10^{-8}. Although the assumed He–Ne laser line position differs slightly from the actual position, all influences from this difference are very small under normal experimental conditions and can be included in a calibration factor. The effectiveness of this formula was verified by correcting an I_2 absorption spectrum collected by using an FTS under similar conditions.

Following this air-to-vacuum correction, conventional calibration was carried out using Ar atomic lines present in our spectra. Standard line positions were taken from the literature (*22*), and the calibration factor was 1.000002119(50).

IV. ANALYSIS

Because the rotational constant of MgBr is relatively small (~0.1 cm^{-1}), and the two dominant isotopomers are almost equally abundant, all of the rotational bands were expected to be very dense and overlapped. For a $^2\Pi$–$^2\Sigma^+$ transition, 8 of 12 branches are spaced approximately by 1*B*. In the initial stage of the assignment, we began with the P_{ff} branch and strong Q_{fe} branch in (0, 0) band because P_{ff} has a 3*B* spacing between each rotational line. Moreover, P_{ff} branch as shown in Fig. 3 was isolated from other strong branches such as Q_{fe} and Q_{ef}.

We utilized the traditional $\mathbf{N}^2$ Hamiltonians of Brown *et al.* (*23*) for our analysis. The matrix elements are listed by Amiot *et al.* for the $^2\Pi$ state (*24*) and by Douay *et al.* for the $^2\Sigma^+$ state (*25*). To start the analysis, we made combination differences between P_{ff} and Q_{fe} branches in each spin component of the (0, 0) band using the averaged molecular constants for the two bromine isotopomers. Based on these preliminary molecular constants for the *A* state, we assigned the lines of the strong Q_{ef} branches. In this step, the molecular constants in ground state were fixed to the values obtained from the microwave data (*16*). The bandhead positions of P_{ff} and Q_{ef} branches were used to estimate the sign and magnitude of the lambda-doubling constant *p*. After recognizing the isotopic splitting in Q_{fe} branches, we fitted the bromine isotopomers separately. If we did not have such severe overlapping, our estimated accuracy for the line positions would be better than 0.01 cm^{-1}. However, because of very severe overlapping in our spectrum, we generally had to assume a value of 0.05 cm^{-1} for the accuracy of the line positions, while 0.01 cm^{-1} was used for the less blended parts of the Q_{fe}, R_{ff}, and R_{ee} branches in the F_2 spin component and the P_{ff} branches in the both spin components. We also included the microwave data (*16*) after correcting for the hyperfine structure of the bromine nuclei.

TABLE 5
Observed and Calculated Relative Intensities of the Q_{ef} Bandheads

$v'\backslash v''$	Ω'	0	1	2	3	4
0	1/2	**1.000 (1.000)**	**0.110 (0.065)**	**0.008 (0.003)**	-	-
		J = 21.5	*J = 17.5*	*J = 14.5*		
	3/2	**0.795 (0.830)**	**0.068 (0.065)**	**0.004 (0.003)**	-	-
		J = 22.5	*J* = 16.5	*J* = 13.5		
1	1/2	**0.021 (0.044)**	**0.548 (0.406)**	**0.103 (0.070)**	**0.010 (0.006)**	-
		J = 28.5	*J = 21.5*	*J = 17.5*	*J = 14.5*	-
2	1/2	-	-	**0.185 (0.150)**	**0.055 (0.052)**	**0.009 (0.007)**
		-	-	*J = 21.5*	*J = 17.5*	*J = 14.5*

Note. Top (bold): observed intensity and calculated intensity at T = 800 K (in parentheses), and bottom (italic): the quantum number *J* of the upper state at the band head. The observed and calculated intensities are relative to the $\Omega' = 1/2$, v = 0 − 0 of Q_{ef} band head. For more details on the calculated values, see the text.

The (0, 1) band was assigned easily using the molecular constants determined from the (0, 0) band and the microwave data for $v = 1$ (*16*). In this assignment, we estimated that the line accuracy was 0.05 cm^{-1} for all lines. Fortrat diagrams in Figs. 5 and 6 summarize the data used in our fitting. To simplify the figures, we removed the P_{ee} and R_{ff} branches. For these two branches, R_{ff} branch was distinct and included in our fit, but the P_{ee} branch was so weak that it was removed from our fit. The line positions are listed in an appendix,[4] and the molecular constants are listed in Table 1. In the final fitting, the Λ-doubling constant q was negligible and thus it was fixed to zero for both isotopomers.

To estimate the vibrational constants for the *A* state, we also measured the bandhead positions for all detected bands. These bandhead positions are listed in Table 2 with their assignment. These heads were converted to band origins for a more reliable vibrational analysis by assuming that the α_e value of the rotational constant in the *A* state was the same as in the ground state. All centrifugal distortion constants and lambda-doubling constants p were fixed to the values for $v = 0$. Because we could not obtain any vibrationally excited heads for the $A^2\Pi_{3/2}$ spin component, we used Harrington's results up to $v_A = 2$ (*12*), corrected on the basis of our observed bandheads. All vibrational constants are summarized in Table 3. These data also allowed us to revise the spin–orbit interaction constants, A_{SO}, for the vibrationally excited levels in the *A* state, $A_1 = 101.416(96)$, $A_2 = 85.553(99)$ cm^{-1}. These data are in good agreement with the data obtained by medium-resolution LIF spectroscopy (*15*).

[4] This appendix is available electrically from the Journal of Molecular Spectroscopy. The full data used in this analysis may also be obtained electronically from authors TH (thirao@sciborg.uwaterloo.ca) or PFB (bernath@UWaterloo.ca).

V. DISCUSSION

The observed molecular constants in Table 1 generally obey the customary mass relationships between the two bromine isotopomers (*26*). MgBr is sufficiently heavy that the Born–Oppenheimer approximation is valid for both the $A^2\Pi$ and $X^2\Sigma^+$ states. The centrifugal distortion constants, however, showed some deviations caused by the severe overlapping of most of the lines. To fix this problem, clean high-resolution spectra containing high *J* transitions such as millimeter-wave or vibration–rotation spectra are required. For this purpose, our results are helpful in predicting the line positions.

The r_0 bond lengths in the *A* state are 2.323644(10), 2.323645(10) Å for $Mg^{79}Br$ and $Mg^{81}Br$, respectively, where the numbers in parentheses indicate three times the standard error. These results compared well with the value of 2.355 Å calculated by Sadygov *et al.* (*15*), and they were about 0.02 Å shorter than the r_e bond length of the ground state (*16*).

According to pure precession theory (*6*), the Λ-doubling constant can be represented by:

$$p = \frac{2A_{SO}Bl(l+1)}{E_\Pi - E_\Sigma}. \qquad [5]$$

In this case, the orbit angular momentum $l = 1$, and the spin–orbit interaction constant A_{SO} of the *A* state is about $+120$ cm^{-1}. The Λ-doubling interaction arises from the interaction between the *A* state and a nearby $^2\Sigma^+$ state. The $D^2\Sigma^+$ states is about 21 600 cm^{-1} above from the *A* state (*27*) and thus the constant p is expected to be negative. However, the Λ-doubling constants of both isotopomers are actually observed to be positive. This discrepancy was also seen in the case of MgCl (*4*, *28*). The electronic configuration of the *A*

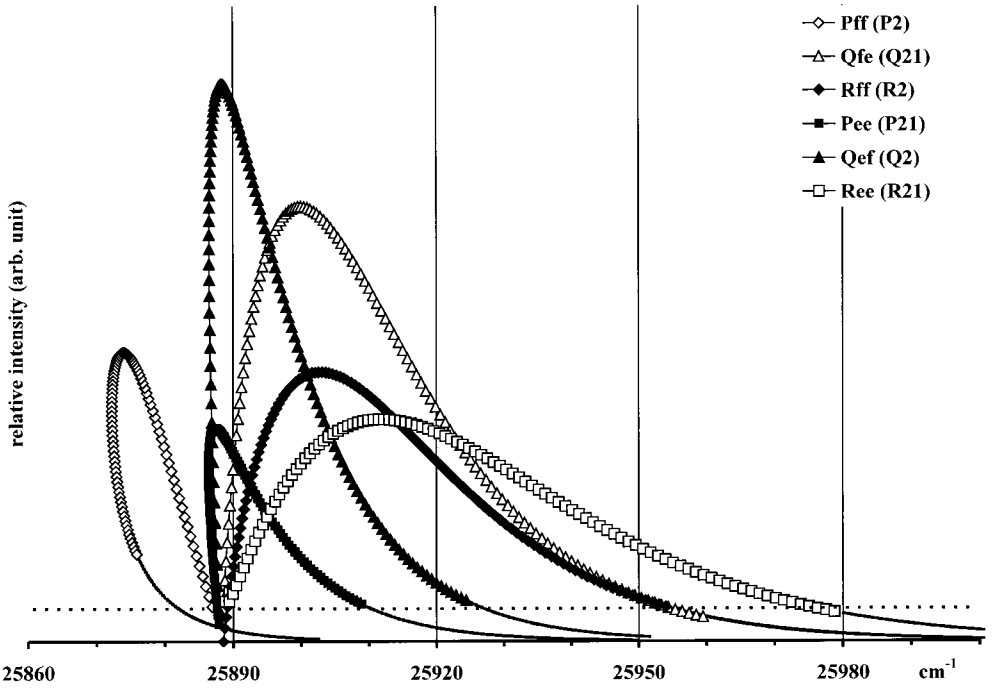

FIG. 7. Calculated intensity distribution of the F_2 spin component of the (0, 0) band. The horizontal and vertical axes indicate observed line position and calculated relative intensity, respectively. To calculate the relative intensity, the temperature was assumed to be 800 K. The transitions indicated by solid lines were not observed in our spectrum. The horizontal, broken line shows the approximate detection limit of our system. For more details, see the text.

state should be represented by the mixture of bound $^2\Pi$ state (regular) and the continuum $^2\Pi$ state (inverted) so the simple formula [5] does not apply.

Vibrational constants of $Mg^{79}Br$ in Table 3 match very well with the theoretical results and the medium-resolution LIF spectra (*15*), as well as the older literature values (*8*). We also calculated the vibrational constants for $Mg^{81}Br$ from those of $Mg^{79}Br$ using the isotope relationship (*1*) and there is good agreement.

By using the vibrational and rotational constants, we calculated the Rydberg–Klein–Rees (RKR) potentials (*29*) and Franck–Condon factors (*30*) to describe the relative intensity of several vibrational bands in the *A–X* transition. In this calculation, we assumed that the observed vibrational levels of the *A* state are not perturbed. The calculated Franck–Condon factors for $Mg^{79}Br$ were listed in Table 4.

The relative intensity, *I*, for each line can be explained by the formula (*6, 31*)

$$I \propto \frac{n_{J'}}{2J' + 1} q_{v'v''} S_{J'J''}, \qquad [6]$$

where $n_{J'}$ is the population in the higher energy level, $q_{v'v''}$ is the Franck–Condon factor, and $S_{J'J''}$ is the Hönl–London factor (*32*). Based on this formula and the Franck–Condon factors in Table 4 and by assuming that all bandheads result from the pile-up of five rotational lines for the Q_{ef} and P_{ee} branches, one can calculate the relative intensity of bandheads (Table 5). In this calculation, we assumed a temperature of 800 K. Sadygov *et al.* (*15*) suggested that the F_2 spin component of the $v = 1$ and 2 vibrational levels in the *A* state are perturbed and they do not emit radiation and the F_1 spin component can be indirectly perturbed through **S**-uncoupling interaction. However, our Franck–Condon factors generally reproduced the relative intensity of bandheads, and thus our results suggest that the F_1 spin component is not perturbed, at least for low *J* levels for $v = 0$, 1, and 2. The *J* values at which the Q_{ef} bandheads occur are provided in Table 5.

At sufficiently high *J* values, indirect predissociation of the F_1 level for $v = 1$ and 2 will be observed because of spin uncoupling. However, we did not see this effect because $v = 1$ and 2 of the $A^2\Pi$ state are well represented by Hund's case (a) coupling for our data. For example (*31*), the value of *BJ* is about 8 cm^{-1} at $J = 50.5$, which is much smaller than the spin–orbit coupling constant A_{SO} of 101 cm^{-1} for $v = 1$ and 85 cm^{-1} for $v = 2$.

In the case of predissociation resonance, sometimes the lifetimes in the *A* state decrease as the quantum number *J* increases, inducing a line broadening in the higher *J* transitions. However, this effect is easier to see in absorption than in emission and we did not see it in our measurements. Instead of seeing a line broadening, we expected to see cutoff in our spectrum. Figure 7 plots the observed lines and their calculated relative intensity for the F_2 spin component. In this calculation, we utilized the Hönl–

London factors provided by Earls (*32*) and assumed a temperature of 800 K. Figure 7 also reveals that the R_{ee}, R_{ff}, and Q_{fe} branches were detected when the intensities were above a threshold (a horizontal broken line), which implies that there was no significant cutoff at a specific J value. However, our vibrational and rotational constants allow us to calculate an upper limit for the dissociation energy of $D_0^0 = 26\,268.4\ \text{cm}^{-1}$. This value is based on the absence of the energy level with $v = 1$, $\Omega = \frac{3}{2}$, $J = 1.5$ in our spectrum. Our value is smaller than the latest *ab initio* value of $D_e = 27\,900\ \text{cm}^{-1}$ (*15*) and a thermochemical value of $D_0^0 = 27\,040\ \text{cm}^{-1}$ (*8*).

VI. SUMMARY

In this study, we recorded emission spectra of the $A^2\Pi$–$X^2\Sigma^+$ system of MgBr by using a Fourier transform spectrometer. A set of rotational and vibrational constants for the two bromine isotopomers were obtained following a rotational analysis of the (0, 0) and (0, 1) bands, and a vibrational analysis of the bandheads up to $v_A = 2$, $v_X = 4$. By using these molecular constants, we obtained RKR potentials and Franck–Condon factors for the A–X transition that reproduced the relative line intensities. This study provides an upper limit of $26\,268.2\ \text{cm}^{-1}$ for the dissociation energy D_0^0 and more information on the predissociation resonance in the A state.

ACKNOWLEDGMENTS

The authors thank Dr. M. Carleer for iodine data and fruitful discussions about Fourier transform spectroscopy. We also thank Professor R. J. Le Roy for the computer programs used to calculate RKR potentials and Franck–Condon factors. T.H. is grateful to Dr. M. Elhanine for encouragement and valuable suggestions about emission measurements with the FTS. This work was supported by the Natural Sciences and Engineering Research Council of Canada (NSERC), and the Killam Foundation. Acknowledgment is also made to the Petroleum Research Fund for partial support.

REFERENCES

1. G. Herzberg, "Molecular Spectra and Molecular Structure, Volume I—Spectra of Diatomic Molecules," 2nd ed., Krieger, Melbourne, FL, 1989.
2. W. J. Balfour, *J. Phys. B: At., Mol. Opt. Phys.* **3,** 1749–1756 (1970).
3. C. M. Olmsted, *Z. Wiss. Phot.* **4,** 293–333 (1906).
4. J. Rostas, N. Shafizadeh, G. Taieb, B. Bourguignon, and M. G. Prisant, *Chem. Phys.* **142,** 97–109 (1990).
5. M. Singh, G. S. Ghodgaonkar, and M. D. Saksena, *Can. J. Phys.* **65,** 1594–1603 (1987).
6. H. Lefebvre-Brion and R. W. Field, "Perturbations in the Spectra of Diatomic Molecules," Academic Press, San Diego, 1986.
7. R. F. Barrow and J. R. Beale, *Proc. Phys. Soc.* **91,** 483–488 (1967).
8. K. P. Huber and G. Herzberg, "Molecular Spectra and Molecular Structure, Volume IV—Constants of Diatomic Molecules," Van Nostrand–Reinhold, New York, 1979.
9. G. Parlent, J. Rostas, G. Taieb, and D. R. Yarkony, *J. Chem. Phys.* **93,** 6403–6418 (1990).
10. O. H. Walters and S. Barratt, *Proc. R. Soc. London Ser. A* **118,** 120–137 (1928).
11. F. Morgan, *Phys. Rev.* **50,** 603–607 (1936).
12. R. E. Harrington, Ph.D. thesis, University of California, 1942.
13. M. M. Patel and P. D. Patel, *J. Phys. B: At., Mol. Opt. Phys.* **2,** 515–516 (1969).
14. S. N. Puri and H. Mohan, *Curr. Sci.* **43,** 442–443 (1974).
15. R. G. Sadygov, J. Rostas, G. Taieb, and D. Yarkony, *J. Chem. Phys.* **106,** 4091–4101 (1997).
16. K. A. Walker and M. C. L. Gerry, *J. Chem. Phys.* **107,** 9835–9841 (1997).
17. E. G. Lee, J. Y. Seto, T. Hirao, P. F. Bernath, and R. J. Le Roy, *J. Mol. Spectrosc.* **194,** 197–202 (1999).
18. F. M. Phelps, III, "M. I. T. Wavelength Tables, Volume 2: Wavelengths by Element," The MIT Press, Cambridge, MA, 1982.
19. B. Edlén, *Metrologia* **2,** 71–80 (1966).
20. K. Birch and M. J. Downs, *Metrologia* **30,** 155–162 (1993).
21. D. R. Lide (Ed.), "Handbook of Chemistry and Physics," 72nd ed., CRC Press, Boca Raton, FL, 1991.
22. G. Norlén, *Phys. Scr.* **8,** 249–268 (1973).
23. J. M. Brown, E. A. Colbourn, J. K. G. Watson, and F. D. Wayne, *J. Mol. Spectrosc.* **74,** 294–318 (1979).
24. C. Amiot, J.-P. Maillard, and J. Chauville, *J. Mol. Spectrosc.* **87,** 196–218 (1981).
25. M. Douay, S. A. Rogers, and P. F. Bernath, *Mol. Phys.* **64,** 425–436 (1988).
26. I. Mills, T. Cvitaš, K. Homann, N. Kallay, and K. Kuchitsu, "Quantities, Units and Symbols in Physical Chemistry," 2nd ed., Blackwell Scientific, Oxford, 1993.
27. V. M. Rao, M. L. P. Rao, and B. R. K. Reddy, *J. Phys. B: At., Mol. Opt. Phys.* **15,** 4161–4163 (1982).
28. (a) R. F. Gutterres, C. E. Fellows, and M. Vervloet, unpublished manuscript; (b) T. Hirao, P. F. Bernath, R. F. Gutterres, C. E. Fellows, and M. Vervloet, in preparation.
29. R. J. Le Roy, "RKR1. A Computer Implementing the First-Order RKR Method for Determining Diatom Potential Energy Curves from Spectroscopic Constants," Univ. Waterloo Chem. Phys. Res. Rep., CP-425, 1992.
30. R. J. Le Roy, "LEVEL 6.1. A Computer Program Solving the Radial Schrödinger Equation for Bound and Quasibound Levels, and Calculating Various Expectation Values and Matrix Elements," Univ. Waterloo Chem. Phys. Res. Rep., CP-555R, 1996.
31. P. F. Bernath, "Spectra of Atoms and Molecules," Oxford Univ. Press, New York, 1995.
32. L. T. Earls, *Phys. Rev.* **48,** 423–424 (1935).